



High Rate Plastic Deformation and Failure of Tungsten-Sintered Metals

by Todd W. Bjerke and William R. Edmanson

ARL-RP-84

September 2004

A reprint from the Proceedings of the 2004 Society for Experimental Mechanics Annual Conference and Exhibition, Costa Mesa, CA, 7–10 June 2004; paper no. 90, session no. 041.

NOTICES

Disclaimers

The findings in this report are not to be construed as an official Department of the Army position unless so designated by other authorized documents.

Citation of manufacturer's or trade names does not constitute an official endorsement or approval of the use thereof.

Destroy this report when it is no longer needed. Do not return it to the originator.

Army Research Laboratory

Aberdeen Proving Ground, MD 21005-5066

ARL-RP-84

September 2004

High Rate Plastic Deformation and Failure of Tungsten-Sintered Metals

**Todd W. Bjerke and William R. Edmanson
Weapons and Materials Research Directorate, ARL**

A reprint from the Proceedings of the 2004 Society for Experimental Mechanics Annual Conference and Exhibition, Costa Mesa, CA, 7–10 June 2004; paper no. 90, session no. 041.

Report Documentation Page

Form Approved
OMB No. 0704-0188

Public reporting burden for this collection of information is estimated to average 1 hour per response, including the time for reviewing instructions, searching existing data sources, gathering and maintaining the data needed, and completing and reviewing the collection information. Send comments regarding this burden estimate or any other aspect of this collection of information, including suggestions for reducing the burden, to Department of Defense, Washington Headquarters Services, Directorate for Information Operations and Reports (0704-0188), 1215 Jefferson Davis Highway, Suite 1204, Arlington, VA 22202-4302. Respondents should be aware that notwithstanding any other provision of law, no person shall be subject to any penalty for failing to comply with a collection of information if it does not display a currently valid OMB control number.

PLEASE DO NOT RETURN YOUR FORM TO THE ABOVE ADDRESS.

1. REPORT DATE (DD-MM-YYYY) September 2004		2. REPORT TYPE Reprint		3. DATES COVERED (From - To) October 2003–March 2004	
4. TITLE AND SUBTITLE High Rate Plastic Deformation and Failure of Tungsten-Sintered Metals				5a. CONTRACT NUMBER	
				5b. GRANT NUMBER	
				5c. PROGRAM ELEMENT NUMBER	
6. AUTHOR(S) Todd W. Bjerke and William R. Edmanson				5d. PROJECT NUMBER 611102.AH42	
				5e. TASK NUMBER	
				5f. WORK UNIT NUMBER	
7. PERFORMING ORGANIZATION NAME(S) AND ADDRESS(ES) U.S. Army Research Laboratory ATTN: AMSRD-ARL-WM-TD Aberdeen Proving Ground, MD 21005-5066				8. PERFORMING ORGANIZATION REPORT NUMBER ARL-RP-84	
9. SPONSORING/MONITORING AGENCY NAME(S) AND ADDRESS(ES)				10. SPONSOR/MONITOR'S ACRONYM(S)	
				11. SPONSOR/MONITOR'S REPORT NUMBER(S)	
12. DISTRIBUTION/AVAILABILITY STATEMENT Approved for public release; distribution is unlimited.					
13. SUPPLEMENTARY NOTES A reprint from the <i>Proceedings of the 2004 Society for Experimental Mechanics Annual Conference and Exhibition</i> , Costa Mesa, CA, 7–10 June 2004; paper no. 90, session no. 041.					
14. ABSTRACT The competition between plastic deformation and brittle fracture during high rate loading of a tungsten-sintered metal is examined through impact experiments, post-experiment microscopy, and numerical simulation. The impact specimens were beam-shaped with a square cross section made from 93% tungsten with a tungsten-nickel-iron binder. The specimens were impacted at the mid-span location with a tungsten striker bar having an initial speed of 55 m/s. Dynamic stretching of the beam rear surface and time of fracture initiation was measured with a strain gage. Strain gage signals indicated that the strain-to-failure was approximately 1.3%, however a significant number of microcracks were observed to have opened underneath the strain gage location. Scanning electron microscopy revealed that brittle “pre-cracking” of the rear surface preceded the ultimate failure of the specimen. A numerical simulation of the impact event was performed using the finite element code ABAQUS to better evaluate the possible role of plastic deformation in the tungsten material prior to failure.					
15. SUBJECT TERMS fracture, dynamic failure, impact					
16. SECURITY CLASSIFICATION OF:			17. LIMITATION OF ABSTRACT	18. NUMBER OF PAGES	19a. NAME OF RESPONSIBLE PERSON
a. REPORT	b. ABSTRACT	c. THIS PAGE			Todd W. Bjerke
UNCLASSIFIED	UNCLASSIFIED	UNCLASSIFIED	UL	12	19b. TELEPHONE NUMBER (Include area code) 410-306-0799

High Rate Plastic Deformation and Failure of Tungsten-Sintered Metals

Todd W. Bjerke, Mechanical Engineer
William R. Edmanson, Mechanical Engineering Technician
U.S. Army Research Laboratory, AMSRL-WM-TD
Aberdeen Proving Ground, Maryland 21005-5069

ABSTRACT

The competition between plastic deformation and brittle fracture during high rate loading of a tungsten-sintered metal is examined through impact experiments, post-experiment microscopy, and numerical simulation. The impact specimens were beam-shaped with a square cross section made from 93% tungsten with a tungsten-nickel-iron binder. The specimens were impacted at the mid-span location with a tungsten striker bar having an initial speed of 55 m/s. Dynamic stretching of the beam rear surface and time of fracture initiation was measured with a strain gage. Strain gage signals indicated that the strain-to-failure was approximately 1.3%, however a significant number of microcracks were observed to have opened underneath the strain gage location. Scanning electron microscopy revealed that brittle "pre-cracking" of the rear surface preceded the ultimate failure of the specimen. A numerical simulation of the impact event was performed using the finite element code ABAQUS to better evaluate the possible role of plastic deformation in the tungsten material prior to failure.

INTRODUCTION

Tungsten-sintered metals, commonly referred to as tungsten heavy alloys or WHA, are a class of material used for anti-armor penetrators. This material consists of tungsten grains surrounded by a matrix alloy such as nickel-iron-tungsten. Fracture can occur as the result of four different mechanisms, decohesion between adjacent tungsten grains, cleavage of tungsten grains, ductile failure of the matrix material, and decohesion of the matrix from the tungsten grains. The material typically has a 90 to 95% tungsten composition (by weight), which gives rise to the potential for a significant number of tungsten grains to be in contact with each other thereby increasing the possibility that decohesion between tungsten grains plays a significant role in material failure.

There have been studies performed in the past to examine the dynamic deformation of tungsten-sintered alloys. Split Hopkinson bar and drop weight tower experiments have been used to examine the rate-dependent constitutive behavior of various composition WHA [1-10]. The general consensus of the various investigations is that the yield stress and ultimate strength of WHA increase with increasing strain rate while the amount of plastic strain decreases with increases in strain rate. Swaging and heat aging have been found to increase the dynamic strength of WHA [2, 10]. The influence of rate and temperature on the failure or fracture of WHA has also been examined. Couque et al. [10] found the fracture toughness of WHA to decrease with increasing loading rate. Rittel and Weisbrod [11] show that the toughness can decrease or increase with increasing loading rate, depending on the orientation of the swaged material microstructure with the applied load. Woodward and O'Donnell [12] identified the crack nucleation and rupture mechanisms for a number of different WHA materials under quasi-static loading conditions and determined the influence of temperature upon these mechanisms [13]. At low temperatures, small microcracks were observed to form from decohesion of adjacent tungsten grains, and eventual rupture of the specimen occurred by the cascading of these microcracks. As specimen temperature was increased, the mechanisms of fracture shifted to one of mixed mechanisms to eventually one of tungsten grain cleavage at the highest temperature examined. This paper describes a study to examine the mechanisms of fracture initiation resulting from impact loading at room temperature. The competition between bulk plastic deformation and brittle microcrack formation is examined through impact experiments, post-experiment microscopy, and numerical simulations.

EXPERIMENTS

The primary issue investigated in this paper is the relative amount of bulk plasticity and microcracking that occur in a WHA material during high rate loading at room temperature. To address this issue, a series of experiments was performed to measure material strain and to determine if microcracks do in fact exist prior to the formation of a large, unstable crack. The

experimental configuration used was a dynamic beam impact test, depicted in Figure 1. The beam-shaped WHA test specimen was struck with a WHA projectile of similar composition to induce a dynamic mode I fracture event initiating on the side opposite that struck by the projectile. A strain gage was placed on the flat surface opposite the impacted face to measure the amount of surface stretching up to the time of fracture and to serve as a crack initiation gage. During dynamic beam flexure but prior to failure, small microcracks that either pre-exist or form during dynamic loading will open, and possibly remain open for post-test inspection. It is through post-test optical inspection of the region near the fracture surface that the existence of microcracks can be verified and their depth determined.

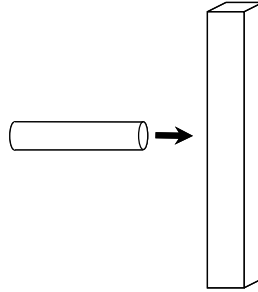


Figure 1. Schematic depiction of the beam impact experiments.

The experiments were performed using a 93% (by weight) tungsten, 5.6% nickel, and 1.4% iron WHA. The bulk density was 17.76 g/cm^3 . The original material was in the form of a bar that had been swaged to 20% reduction in area and aged. The quasi-static ultimate tensile true stress was 1.425 GPa, the logarithmic failure strain was 12.5%, and the quasi-static yield stress was 1.19 GPa (these were furnished by the material supplier). The dilatational and shear wave speeds were measured to be 5163 and 2824 m/s using an ultrasound technique. The elastic modulus and Poisson's ratio were 365 GPa and 0.29, respectively. These were determined from the measured wave speeds. Beam specimens were cut from a large WHA bar using conventional machining techniques. The beam specimen had a length of 127 mm and a square cross section with height and width of 9 mm each. The length and diameter of the striking projectile were 44.5 and 8.9 mm, respectively. The impact speed was 55 m/s for each of the 8 experiments performed. The strain gage mounted on the face opposite that impacted by the projectile was placed where the macroscopic crack would initiate. The gage had an active grid length of 3.2 mm and was connected to a 1 MHz-bandwidth signal conditioning amplifier and a 500 MHz digital storage oscilloscope. Crack initiation caused the strain gage to split into two pieces, resulting in the strain signal to saturate. This feature of the strain gage signal provided a crack initiation time. The time of projectile contact with the beam specimen was measured with a "make circuit" where the electrically conducting projectile completes an electrical circuit on the impact face of the fracture specimen. This also served as a reliable trigger for the oscilloscope.

The strain gage signal for a typical impact experiment is shown in Figure 2 as the red curve. The time $t = 0$ demarks initial projectile contact with the beam. Wave propagation resulting from the impact is evident in the strain gage signal. The strain gage system responded to a small amount of electromagnetic field generation from the projectile launcher device during the first several microseconds. Fracture was observed to occur when the rear surface strain was 1.3%. This value was consistent among all of the experiments. The typical strain rate of the rear surface near the fracture region was 10^3 s^{-1} .

The rear surface region of the impacted beam specimens near the fracture plane was examined with a scanning electron microscope to establish the presence of microcracks and to estimate microcracking depth. Much of this region was covered by the strain gage during the experiment. To visually examine this area, the remnants of the strain gage were carefully removed. Two typical images of this region are shown in Figure 3. The fracture plane is located just beyond the bottom of the image in Fig. 3(a), and is the bottom portion of Fig. 3(b). Significant microcracking is evident, with the microcracks oriented perpendicular to the beam longitudinal axis. The maximum crack opening was determined to be approximately $1.7 \text{ }\mu\text{m}$. Images of the beam surface taken far from the region of fracture (not shown) did not show any evidence of microcracking, suggesting that the large tensile stress near the fracture plane of the beam was responsible for either opening existing microcracks or causing them to form.

The depth of microcracking was estimated from additional micrographs taken along the region where the macroscopic fracture event initiated. Figure 4 shows the typical surface topography for this region. The beam specimen was rotated into the plane of the image by 40 degrees to obtain the necessary perspective to estimate microcracking depth. The circled area of Fig. 4 shows the remnants of a microcrack. As can be seen, the microcrack has a depth of one tungsten grain, or approximately $40 \text{ }\mu\text{m}$. The formation of microcracks in a tungsten-sintered alloy during tensile loading was discussed in detail by Weerasooriya [9] and Woodward and O'Donnell [12], who found the grain-to-grain contact to be the weakest portion of the alloy and therefore the first to fail. An identical mechanism is likely responsible for the microcracking observed in the recovered beam specimens. The impact experiments verify that microcracks can exist in room temperature tungsten-sintered alloys when subjected to high-rate tensile loads. Furthermore, microcracking appears to penetrate to a depth of one grain diameter below the machined surface.

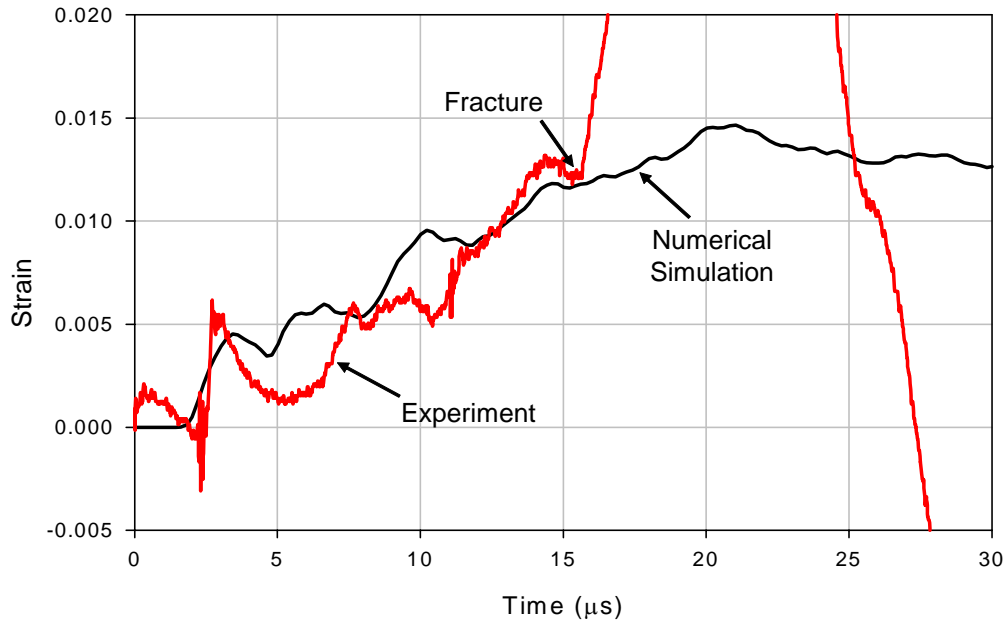


Figure 2. Typical strain gage signal showing surface stretching and crack initiation.

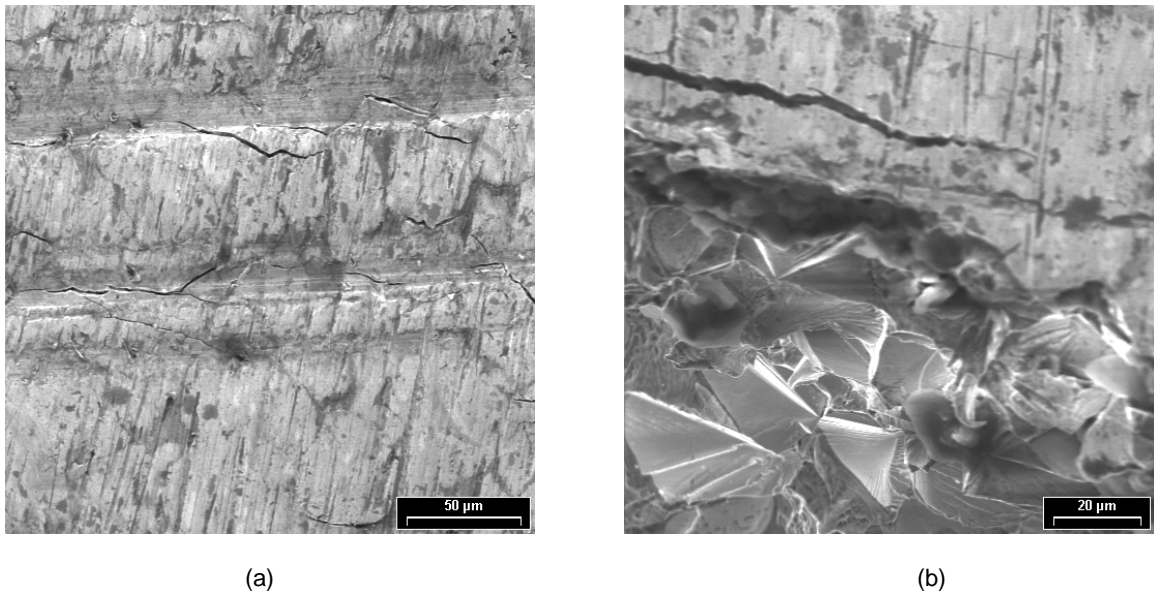


Figure 3. Scanning electron microscope image of the beam specimen. (a) Surface near the fracture plane. Actual fracture plane is located just beyond the bottom of the image. Image was taken normal to the machined surface. (b) Oblique view of a main fracture plane and specimen rear surface. Specimen was rotated 30 degrees to permit inspection of the fracture plane (bottom portion of figure) and initiation site. Further microcracking is evident on the upper portion of the figure.

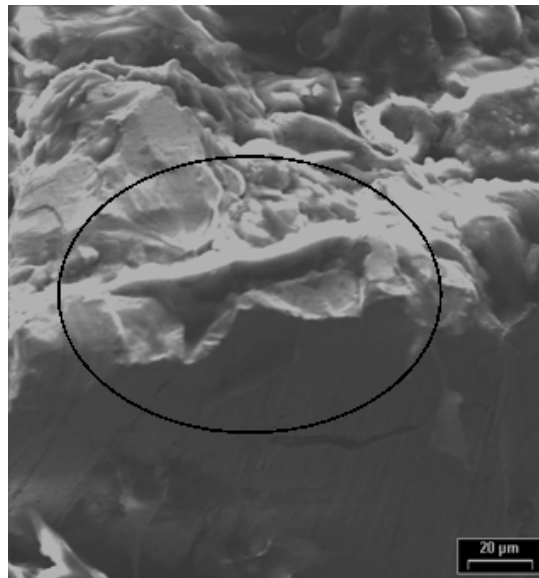


Figure 4. Scanning electron microscope image of a microcrack interacting with the main fracture plane. Circled region identifies the microcrack of interest that extends 40 μm below the surface. Fracture surface is top portion of image.

NUMERICAL SIMULATIONS

A numerical simulation of the beam impact experiments was made using the finite element code ABAQUS. The approach taken was to duplicate the dynamic loading conditions up to the time of crack initiation, at which time the simulation was halted. The crack was never permitted to grow, eliminating the intricacies associated with surface creation in a computational environment. The numerical simulation was used to determine the state of the material on the beam rear surface up to the time of crack initiation. Results from the simulation were then compared to the strain gage signals discussed earlier. Since stretching of the beam rear surface is limited to elastic and plastic deformations in the simulation, an assessment of the relative amount of plastic deformation and microcracking can be made by comparing simulation and experimental results.

A three-dimensional finite element model duplicating the experimental configuration was constructed within ABAQUS CAE. Because the geometry has a plane of symmetry (a vertical plane for the configuration shown in figure 1), only half of the beam specimen and striking projectile were modeled. A boundary condition was imposed along the plane of symmetry that prevented nodes along the symmetry plane from moving perpendicular to the plane. Hexagonal brick-shaped, 8-node elements were used throughout the whole model. A nearly constant element size of 0.5 mm was used. ABAQUS was used in an explicit mode with the inertia of the specimen providing the only support. The interface between the projectile and fracture specimen was modeled as a frictionless contact interface.

The WHA material was modeled as a rate-dependent elastic-plastic material with strain hardening. An elastic modulus of 365 GPa and a Poisson's ratio of 0.29 were used. The quasi-static yield stress for this alloy was 1.19 GPa. Plastic hardening to a true stress of 1.425 GPa was reported by the material supplier. The logarithmic plastic strain at this stress was approximately 12.5%. The rate dependence of the yield stress was obtained from Weerasooriya [9], where a similar WHA swaged 17% was evaluated. Because the material for this study was swaged 20%, a correction was made to the stress levels given by Weerasooriya to correspond to those appropriate for the material of this study. The change in yield stress with strain rate was assumed to be identical to that found in Weerasooriya [9]. It should be noted that the strain rates that occur near the fracture plane were measured during the experiments to be approximately $1,000 \text{ s}^{-1}$. The highest rate reported by Weerasooriya [9] was 750 s^{-1} . It was assumed that the rate dependence given by Weerasooriya was valid for the higher rates encountered in this study. The high-rate stress hardening curve was kept parallel to the quasi-static curve reported by the material supplier.

Results from the numerical simulation are shown in Figure 2 as the opening logarithmic strain history at the mid-span location of the beam. The strain history of the element next to the plane of symmetry was selected because this was identical to where the strain gage was placed. The strain signal shows the presence of stress waves propagating back and forth in the beam and generally follows the same trend as the strain gage from the experiments. The strain at the time of crack initiation was found to be approximately 1.3%, similar to the experimental findings. Although the general trends of the results from the numerical simulation and experiments agree, there are differences in their details. The strain gage signal shows large variations in strain, whereas the numerical simulation shows a general increase in strain with small oscillations. To determine if this could be due to mesh size, an additional simulation was performed with an element size of approximately 0.25 mm, half

the size used to obtain the results in Fig. 2. Identical results were obtained, indicating that the mesh used for the finite element model was of sufficient resolution. The primary discrepancy between experimental and numerical results is thus likely due to surface microcracking, a phenomenon not captured in the finite element model.

DISCUSSION

The beam impact experiments indicated that a macroscopic crack would occur when surface strain approached 1.3%. Post-test inspection of the beam showed significant microcracking to exist in this region. This leads to the question of how much of the strain gage signal was due to the opening of surface microcracks, and how much was due to plastic deformation. An estimate of the surface strain due to microcracking can be made by measuring the amount of microcrack opening at the strain gage location. This was done using scanning electron microscope images such as that shown in Fig. 3(a). The height of the image was used as the gage length for the strain calculation. The total amount of microcrack opening was measured along numerous vertical paths. Accurate crack opening measurements were obtained with supplemental images of considerably higher magnification. The apparent strain in the strain gage region due to microcracking was determined to be approximately 1.0%. The maximum amount of elastic strain the material can support is 0.3% (obtained from the elastic modulus and the yield point). The sum of these two values is equivalent to the total strain, or surface stretching, recorded by the strain gage. Thus, it appears that the strain gage signal is the result of elastic strain and microcrack opening. The numerical simulation indicated that a strain of 1.3% resulting from elastic and plastic deformation would occur at the time of crack initiation. Given the observed presence of extensive surface microcracks, it can be concluded that the surface stretching that occurs in the vicinity of the macroscopic crack is the result of elastic deformation and microcrack opening, not plastic deformation. This also provides a reason for the discrepancy in strain history details between the experiments and the numerical simulation.

The initiation of the macroscopic crack appears to be the result of decohesion of adjacent tungsten grains. Inspection of the fracture surfaces showed microcracks that extended one tungsten grain diameter below the rear surface of the beam specimen. It is speculated that the exact crack initiation site was where there was a fortuitous alignment of tungsten grains that permitted a linear microcrack to extend more than one tungsten grain diameter below the surface. All other microcracks were prevented from growing because they encountered a tungsten grain that blocked their forward path. To progress further, these microcracks would need to either change direction away from the principal loading axis or proceed through a tungsten grain or matrix material, both of which likely require considerably more energy than that needed for decohesion of adjacent tungsten grains. It should be noted that the microcracking resulting from high-rate loading reported here is similar to that observed by O'Donnell and Woodward [13] for quasi-static loading at low-temperature, suggesting that a time-temperature superposition may apply for this class of material.

CONCLUSIONS

A beam impact experimental configuration was used to verify the opening of microcracks in the high stress region of a 93% tungsten-sintered alloy. The microcracks, resulting from decohesion of adjacent tungsten grains, were found to extend below the beam surface approximately one tungsten grain diameter. A strain gage placed on the beam surface recorded a maximum strain prior to specimen fracture of 1.3%. A finite element simulation of the experiment that did not include the physics of microcrack formation but did include a rate-dependent plasticity model also gave a maximum strain of 1.3%. However, details of the finite element strain history did not agree very well with the strain gage signal. Post-test examination of the beam surface where the strain gage was located indicated that the microcracking accounted for 1.0% of the strain, with the remaining 0.3% due to elastic deformation. Given the strain measurements and the observed presence of extensive surface microcracks, it is concluded that the surface stretching that occurs in the vicinity of the macroscopic crack is the result of elastic deformation and microcrack opening, not plastic deformation.

REFERENCES

1. Lee, W.S., Xie, G.L., and Lin, C.F., The strain rate and temperature dependence of the dynamic impact response of tungsten composite. *Materials Science and Engineering A257*, 256-267, 1998.
2. Kim, D.K., Lee, S., and Noh, J.W., Dynamic and quasi-static torsional behavior of tungsten heavy alloy specimens fabricated through sintering, heat-treatment, swaging and aging. *Materials Science and Engineering A247*, 285-294, 1998.
3. Zhang, B.P., Ding, C., Liu, B., Jiao, T., and Zhou, S.H., Dynamic tensile behavior of 93wt.% tungsten alloy and its fractal features of fracture. *Journal de Physique IV 7*, C3-409 – C3-414, 1997.
4. Woodward, R.L., Baldwin, N.J., Burch, I., and Baxter, B.J., Effect of strain rate on the flow stress of three liquid phase sintered tungsten alloys. *Metallurgical Transactions A*, vol. 16A, 2031-2037, 1985.

5. Zhou, M. and Clifton, R.J., Dynamic constitutive and failure behavior of a two-phase tungsten composite. *Journal of Applied Mechanics*, vol. 64, 487-494, 1997.
6. Satapathy, S., Cazamias, J., Bless, S., Gee, R., Meyer, L., and Brar, S., Dynamic strength of tungsten-nickel-cobalt alloys. Institute for Advanced Technology at the University of Texas at Austin Technical Report IAT.P.0345, June 1999.
7. Lankford, J., Couque, H., Bose, A., and German, R., Dynamic deformation and failure of tungsten heavy alloys. *Tungsten and Tungsten Alloys – Recent Advances*. Edited by Andrew Crowson and Edward Chen, The Minerals, Metals, and Materials Society, 151-159, 1991.
8. Weerasooriya, T., Deformation behavior of 93W-5Ni-2Fe at different rates of compression loading and temperatures. U.S. Army Research Laboratory Technical Report ARL-TR-1719, July 1998.
9. Weerasooriya, T., Deformation and failure of a tungsten heavy alloy under tensile loading at different strain rates. *Proceedings of the 2003 Society for Experimental Mechanics Annual Conference and Exposition on Experimental and Applied Mechanics*, Charlotte, North Carolina, June 2-4, 2003.
10. Couque, H., Lankford, J., and Bose, A., Tensile fracture and shear localization under high loading rate on tungsten alloys. *Journal de Physique III*, vol. 2, 2225-2238, 1992.
11. Rittel, D. and Weisbrod, G., Dynamic fracture of tungsten heavy alloys. *International Journal of Fracture*, vol. 112, 87-98, 2001.
12. Woodward, R.L. and O'Donnell, R.G., Tensile rupture of tungsten alloys by the cascade of crack nucleation events. *Journal of Material Science*, vol. 35, 4067-4072, 2000.
13. O'Donnell, R.G. and Woodward, R.L., Influence of temperature on the fracture of a W-Ni-Fe alloy. *Journal of Material Science*, vol. 35, 4319-4324, 2000.

NO. OF
COPIES ORGANIZATION

1 DEFENSE TECHNICAL
(PDF INFORMATION CTR
ONLY) DTIC OCA
8725 JOHN J KINGMAN RD
STE 0944
FT BELVOIR VA 22060-6218

1 COMMANDING GENERAL
US ARMY MATERIEL CMD
AMCRDA TF
5001 EISENHOWER AVE
ALEXANDRIA VA 22333-0001

1 INST FOR ADVNCD TCHNLGY
THE UNIV OF TEXAS
AT AUSTIN
3925 W BRAKER LN STE 400
AUSTIN TX 78759-5316

1 US MILITARY ACADEMY
MATH SCI CTR EXCELLENCE
MADN MATH
THAYER HALL
WEST POINT NY 10996-1786

1 DIRECTOR
US ARMY RESEARCH LAB
IMNE AD IM DR
2800 POWDER MILL RD
ADELPHI MD 20783-1197

3 DIRECTOR
US ARMY RESEARCH LAB
AMSRD ARL CI OK TL
2800 POWDER MILL RD
ADELPHI MD 20783-1197

3 DIRECTOR
US ARMY RESEARCH LAB
AMSRD ARL CS IS T
2800 POWDER MILL RD
ADELPHI MD 20783-1197

NO. OF
COPIES ORGANIZATION

ABERDEEN PROVING GROUND

1 DIR USARL
AMSRD ARL CI OK TP (BLDG 4600)

NO. OF
COPIES ORGANIZATION

ABERDEEN PROVING GROUND

20 DIR USARL
AMSRD ARL WM TD
T BIERKE